A Density Functional Study of [2+3] versus [2+2] Addition of Ethylene to Chromium−Oxygen Bonds in Chromyl Chloride

Maricel Torrent,[†] Liqun Deng,[‡] and Tom Ziegler*[,‡]

Departments of Chemistry, University of Girona, Girona, Catalonia, Spain, and University of Calgary, Calgary, Alberta T2N 1N4, Canada

Received July 18, 1997

Density functional theory (DFT) calculations have been carried out on the [2+2] and [2+3] addition of ethylene to Cr═O bonds in CrO_2Cl_2. The [2+3] addition was found to be more favorable with an electronic reaction enthalpy of −9.6 kcal/mol and an activation barrier of 15.8 kcal/mol. The corresponding values for the [2+2] addition were 15.4 and 27.9 kcal/mol, respectively. It was concluded that epoxides formed in the reaction between CrO_2Cl_2 and olefins are unlikely to originate from a [2+2] addition path to a Cr═O bond as previously suggested. The two addition reactions were analyzed by the intrinsic reaction coordinate method, and comparisons were made to a previous study of [2+2] and [2+3] addition by ethylene to OsO_4. Qualitative considerations were used to rationalize why the addition of ethylene to metal−oxygen bonds in tetrahedral d^0 oxo complexes seems more prone to proceed by a [2+3] mechanism.

Introduction

Transition metal oxides and halides are applied extensively as oxidants in processes where oxygen or halogen is inserted into a C−H linkage or added to an olefin double bond.[1−6] Oxidation carried out in this way is often relatively gentle and remarkably specific compared to the direct application of elemental oxygen or halogen. Many of the oxidation processes have been subject to mechanistic studies.[7−16]

Scheme 1

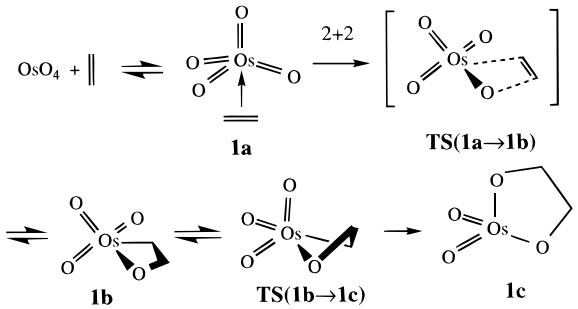

In the reaction with olefins, a number of systems including molybdenum(VI) complexes,[2] permanganate,[3] ruthenium tetraoxide,[4] and osmium tetraoxide[5] produce as the primary products diols.[7,8] At least in the case of OsO_4, two different mechanistic hypotheses have been proposed, namely a [2+2] cycloaddition pathway by Sharpless,[15] Scheme 1, and a [2+3] reaction path by Corey,[16] Scheme 2. Both mechanisms lead to the formation of a metallaoxethane intermediate, **1c**, from which the diol is eliminated by hydrolysis.

[†] University of Girona.
[‡] University of Calgary.

(1) (a) *Organic Synthesis by Oxidation with Metal Compounds*; Mijs, W. J., de Jonge, C. R. H. I., Eds.; Plenum: New York, 1986. (b) Cook, G. K.; Mayer, J. M. *J. Am. Chem. Soc.* **1995**, *117*, 7139. (c) Cook, G. K.; Mayer, J. M. *J. Am. Chem. Soc.* **1994**, *1160*, 1855. (d) Sharpless, K. B.; Akashi, K. *J. Am. Chem. Soc.* **1975**, *97*, 5927. (e) Mosher, W. A.; Celeste, J. R. *Rev. Chim., Acad. Repub. Pop. Roum.* **1962**, *7*, 1085. (f) Hartford, W. H.; Darrin, M. *Chem. Rev.* **1958**, *58*, 1.
(2) Ishii, Y.; Yamawaiki, K.; Yoshida, T.; Ura, T.; Ogawa, M. *J. Org. Chem.* **1987**, *52*, 1868.
(3) Carey, F. A.; Sundberg, R. J. *Advanced Organic Chemistry*; Plenum Press: New York, 1977.
(4) (a) Lee, D. G. In *Oxidation in Organic Chemistry*; Trahanovsky, W. S., Ed.; Academic Press: New York, 1973; Part B. (b) Lee, D. G.; Van den Engh, M. *Can. J. Chem.* **1972**, *50*, 3129.
(5) Singh, H. K. In *Cytochrome P-450: Structure, Mechanism, and Biochemistry*; Ortiz de Montellano, P. R., Ed.; Plenum: New York, 1986.
(6) Sharpless, K. B.; Teranishi, A. Y.; Bäckvall, J. E. *J. Am. Chem. Soc.* **1977**, *99*, 3120.
(7) (a) Stewart, R. In *Oxidation in Organic Chemistry*; Wiberg, K. B., Ed.; Academic Press: New York, 1965; Part A, pp 1−68. (b) House, H. O. Modern Synthetic Reactions; Benjamin: Menlo Park, CA, 1972; pp 257−291. (c) Walba, D. M.; Wand, M. D.; Wilkes, M. C. *J. Am. Chem. Soc.* **1979**, *101*, 4398. (d) Baldwin, J. E.; Crossley, M. L.; Lehtonen, E. M. *J. Chem. Soc., Chem. Commun.* **1979**, 918. (e) Klein, E.; Rojahn, W. *Tetrahedron* **1965**, *21*, 2353.
(8) (a) Schröder, M. *Chem. Rev.* **1980**, *80*, 107. (b) Sharpless, K. B.; Chong, C. A.; Oshima, K. J. *J. Org. Chem.* **1976**, *41*, 177. (c) Herranz, E.; Sharpless, K. B. *J. Org. Chem.* **1978**, *43*, 2544. (d) Herranz, E.; Biller, S. A.; Sharpless, K. B. *J. Am. Chem. Soc.* **1978**, *100*, 3596. (e) Herranz, E.; Sharpless, K. B. *J. Org. Chem.* **1980**, *45*, 2710.
(9) Stairs, R. A.; Diaper, D. G. M.; Gatzke, A. L. *Can. J. Chem.* **1963**, *41*, 1059.
(10) Sharpless, K. B.; Teranishi, A. Y. *J. Org. Chem.* **1973**, *38*, 185.
(11) (a) Cristol, S. J.; Eilar, K. R. *J. Am. Chem. Soc.* **1950**, *72*, 4353. (b) Freeman, F. *Rev. React. Species Chem. React.* **1973**, *1*, 37.
(12) (a) Bachelor, F. W.; Cheriyan, U. O. *Tetrahedron Lett.* **1973**, 3291. (b) Bachelor, F. W.; Cheriyan, U. O. *J. Chem. Soc., Chem. Commun.* **1973**, 195.
(13) (a) Rappé, A. K.; Goddard, W. A., III. *J. Am. Chem. Soc.* **1982**, *104*, 3287. (b) Rappé, A. K.; Goddard, W. A., III. *J. Am. Chem. Soc.* **1980**, *102*, 5115. (c) Rappé, A. K.; Goddard, W. A., III. *J. Am. Chem. Soc.* **1982**, *104*, 448.
(14) Corey, E. J.; Noe, M. C. *J. Am. Chem. Soc.* **1993**, *115*, 12579.
(15) (a) Norrby, P. O.; Kolb, H. C.; Sharpless, K. B. *Organometallics* **1994**, *13*, 344. (b) Norrby, P. O.; Becker, H.; Sharpless, K. B. *J. Am. Chem. Soc.* **1996**, *118*, 35.
(16) (a) Corey, E. J.; Noe, M. C. *J. Am. Chem. Soc.* **1996**, *118*, 319. (b) Corey, E. J.; Noe, M. C.; Grogan, M. J. *Tetrahedron Lett.* **1996**, *37*, 4899.

S0020-1669(97)00896-3 CCC: $15.00
Published on Web 02/26/1998

Scheme 2

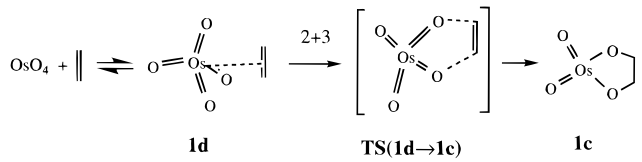

Scheme 3

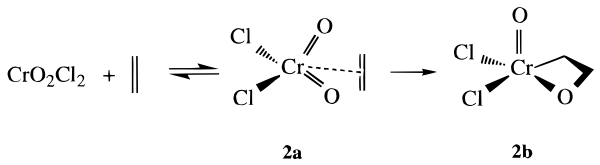

Very recently, several theoretical studies analyzed these two mechanisms for the $OsO_4 + C_2H_4$ reaction.[17a,18,19] They all concluded that the reaction pathway is unlikely to proceed through a [2+2] transition structure involving a four-membered metallacycle, TS(**1a**→**1b**) of Scheme 1, due to the high barrier (∼40 kcal/mol) associated with this path. By contrast, the [2+3] mechanism which invokes a five-membered ester type transition state, TS(**1d**→**1c**) of Scheme 2, appears to be much more feasible with a barrier of a few kilocalories per mole.

Diols seem not to be a product in the reaction of chromyl chloride,[1] CrO_2Cl_2, and olefins. Instead an often complex mixture is produced,[6] with epoxides and *cis*-chlorohydrin as the main products. An early mechanism for olefin oxidation by CrO_2Cl_2 involved the electrophilic attack of $[CrO_2Cl]^+$ on the carbon−carbon double bond. However this mechanism failed[9,10] to explain all stereochemical aspects and was replaced with a mechanism based on [2+3] cis addition[6,9,11,12] as in the case of the metal oxides discussed above. Alternatively, Sharpless et al.[6] have suggested that a [2+2] addition of the carbon−carbon double bond to the metal−oxygen linkage might be at work as the initial step for the oxidation of olefins by CrO_2Cl_2, Scheme 3, in analogy with the corresponding reaction involving OsO_4, Scheme 1. The four-membered metallacycle, **2b** of Scheme 3, formed from the addition of olefin to CrO_2Cl_2 might in subsequent steps rearrange to the observed products such as epoxides.

Support for the importance of [2+2] addition in the oxidation of olefins by CrO_2Cl_2 was later provided by Goddard et al.[13] in a pioneering theoretical study of alkene oxidation. These authors suggested that oxidants such as OsO_4 and MnO_4^- afford diols in reactions with olefins because the five-membered metallaoxethane intermediate, **1c** of Scheme 2, for these species is more stable than the four-membered metallacycle **1b** of Scheme 1. On the other hand, in the case of CrO_2Cl_2 the relative energies of the two ring systems are reversed, with the four-membered metallacycle **2b** of Scheme 3 being the most stable. As a result, CrO_2Cl_2 affords epoxides and other products from a rearrangement of **2b**, rather than diols. Unfortunately, due to limitations in methodology and computational facilities at the time, Goddard et al.[13] were unable to fully optimize the geometrical structures of the different species involved in Scheme 3.

We shall in the present investigation study the [2+2] addition of ethylene to a Cr═O bond, eq 1, as well as the [2+3] addition, eq 2, of ethylene to the two terminal oxygen atoms. Both reaction paths will be traced by the intrinsic reaction coordinate (IRC) method.

$$CrO_2Cl_2 + C_2H_4 \rightarrow TS_1^{\ddagger}([2+2]) \rightarrow Cr(OCl_2)OC_2H_4 \quad (1)$$

$$CrO_2Cl_2 + C_2H_4 \rightarrow TS_2^{\ddagger}([2+3]) \rightarrow Cr(Cl_2)O_2C_2H_4 \quad (2)$$

The objective here has been to test whether the unique product distribution from the reaction between CrO_2Cl_2 and C_2H_4 could be explained in terms of the preference for a [2+2] addition, as suggested by Sharpless.[6] Thus, the [2+2] addition might still be viable for CrO_2Cl_2 although recent theoretical calculations[17a,18,19] showed that it is highly unfavorable for OsO_4. In fact, Rappé[13] and Goddard found in their early calculations that the [2+2] addition of C_2H_4 to CrO_2Cl_2 was exothermic by −14 kcal/mol whereas the corresponding [2+3] cycloaddition was endothermic by 10 kcal/mol.

A second aim of this study has been to analyze the factors determining the relative feasibility of the [2+2] and [2+3] additions of ethylene to CrO_2Cl_2, eqs 1 and 2, as well as OsO_4, eqs 3 and 4. Our analysis will be concerned with the activation

$$OsO_4 + C_2H_4 \rightarrow TS_3^{\ddagger}([2+2]) \rightarrow Os(O_3)OC_2H_4 \quad (3)$$

$$OsO_4 + C_2H_4 \rightarrow TS_4^{\ddagger}([2+3]) \rightarrow Os(O_2)O_2C_2H_4 \quad (4)$$

energies as well as the reaction enthalpies. The detailed IRC studies should further detect possible differences in the mode of attack by ethylene on OsO_4 and CrO_2Cl_2 along the [2+2] and [2+3] reaction paths.

Computational Details

The reported calculations were carried out by using the Amsterdam Density Functional (ADF) package developed by Baerends et al.[20] and vectorized by Ravenek.[21] The adopted numerical integration procedure was due to te Velde et al.[22] A set of auxiliary s, p, d, f, and g STO functions, centered on all nuclei, were introduced in order to fit the molecular density and Coulomb potential accurately in each SCF cycle.[23] An uncontracted triple-ζ STO basis set was employed for the *n*s, *n*p, *n*d, $(n + 1)$s, and $(n + 1)$p valence orbitals of the transition metal elements. For carbon (2s,2p), oxygen (2s,2p), chlorine (3s,3p), and hydrogen (1s), use was made of a double-ζ basis set augmented by an extra polarization function.[24] The fully occupied inner shells of chlorine and chromium (1s2s2p), as well as carbon and oxygen (1s), were assigned to the cores and treated by the frozen-core approximation.[25] All the geometries and frequencies were calculated at the local

(17) (a) Torrent, M.; Deng, L.; Duran, M.; Solà, M.; Ziegler, T. *Organometallics* **1997**, *16*, 13. (b) Seip, H. M.; Stolevik, R. *Acta Chem. Scand.* **1966**, *20*, 385. (c) Marsden, C. J.; Hedberg, K. *Inorg. Chem.* **1982**, *21*, 1115.
(18) Dapprich, S.; Ujaque, G.; Maseras, F.; Lledós, A.; Musaev, D. G.; Morokuma, K. *J. Am. Chem. Soc.* **1996**, *118*, 11660.
(19) (a) Pidun, U.; Boehme, C.; Frenking, G. *Angew. Chem., Int. Ed.* Engl. **1996**, *35*, 2817. (b) DelMonte, A. J.; Haller, J.; Houk, K. H.; Sharpless, K. B.; Singleton, D. A.; Strassner, T.; Thomas, A. A. *J. Am. Chem. Soc.* **1997**, *119*, 9907.
(20) Baerends, E. J.; Ellis, D. E.; Ros, P. *Chem. Phys.* **1973**, *2*, 41.
(21) Ravenek, W. In *Algorithms and Applications on Vector and Parallel Computers*; te Riele, H. J. J., Dekker, T. J.; van de Vorst, H. A., Eds.; Elsevier: Amsterdam, 1987.
(22) (a) Boerrigter, P. M.; te Velde, G.; Baerends, E. J. *Int. J. Quantum Chem.* **1987**, *33*, 87. (b) te Velde, G.; Baerends, E. J. *J. Comput. Phys.* **1992**, *99*, 84.
(23) Krijn, J.; Baerends, E. J. *Fit Functions in the HFS-methods*; Internal Report; Free University of Amsterdam: Amsterdam, 1984.
(24) (a) Snijders, G. J.; Baerends, E. J.; Vernooijs, P. *At. Nucl. Data Tables* **1982**, *26*, 483. (b) Vernooijs, P.; Snijders, G. J.; Baerends, E. J. *Slater Type Basis Functions for the Whole Periodic System*; Internal Report; Free University of Amsterdam: Amsterdam, 1981.
(25) (a) Snijders, G. J.; Baerends, E. J.; Ros, P. *Mol. Phys.* **1978**, *36*, 1789. (b) Snijders, G. J.; Baerends, E. J.; Ros, P. *Mol. Phys.* **1979**, *38*, 1909.

density approximation (LDA) level[26] with the parametrization of Vosko et al.[27] The relative energies were evaluated by including Becke's nonlocal exchange[28] and Perdew's nonlocal correlation corrections[29] as perturbations based on the LDA density. This approach is denoted NL-P, and its validity has been discussed elsewhere.[30] The geometry optimization procedure was based on an analytical gradient scheme developed by Versluis and Ziegler,[31a] Fan and Ziegler,[31b] and Schreckenbach[31c] et al. The harmonic vibrational frequencies were computed from the force constants obtained by numerical differentiation of the energy gradients.[32] For the osmium system, relativistic corrections to the total energy were taken into account by the quasi-relativistic method (QR).[33a,b] The application of this scheme, in comparison to other relativistic methods, has been discussed by Li et al.[33] The transition state structures were located by a series of constrained geometry optimization in which the bonds formed and broken were fixed at various lengths while the remaining internal coordinates were optimized. The approximate stationary points located from such a procedure were then fully optimized using the standard transition state optimization procedure with an algorithm due to Banerjee et al.[34] and Baker [35] in the ADF implementation due to Fan et al.[36] All first-order saddle points were shown to have a Hessian matrix with a single negative eigenvalue. The reaction pathways were traced by the intrinsic reaction coordinate (IRC) method due to Fukui[37] based on a search scheme by González and Schlegel[38] and incorporated into the ADF program by Deng and Ziegler.[39]

Results and Discussion

We shall now turn to a full discussion of the reaction path for the [2+2] and [2+3] additions of ethylene the Cr−O bonds in CrO_2Cl_2. The first sections, A−C, will be devoted to the geometrical features of the stationary points and the structural changes along the reaction paths. A complete discussion of the energy profile for the processes will be given later in section D whereas sections E and F provide an analysis of the calculated results in terms of qualitative molecular orbital theory.

A. Geometries of the Reactants and Products. Figure 1 displays the optimized geometries for the CrO_2Cl_2 reactant, **3**, as well as the [2+2], **4**, and [2+3], **5**, products from the reactions in eqs 1 and 2. Frequency calculations confirmed that the structures reported all represent energy-minimum points. All structures were optimized without symmetry constraints.

The reactant CrO_2Cl_2, **3**, is a d^0 complex with a singlet ground state. It was optimized to have C_{2v} symmetry in agreement with experiment.[17c] The optimized distances of R(Cr−Cl) = 2.104 Å and R(Cr−O) = 1.571 Å are in good agreement with the experimental[17c] estimates of R(Cr−Cl) = 2.126 (2) Å and R(Cr−O) = 1.581 (2) Å, respectively, whereas the optimized

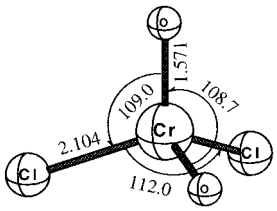

3

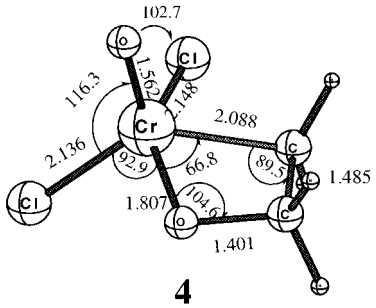

4

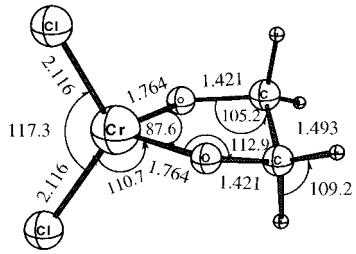

5

Figure 1. Optimized geometries of the reactant CrO_2Cl_2 (**3**), the four-member product (**4**) from the [2+2] cycloaddition of C_2H_4 to the Cr═O bond of CrO_2Cl_2 in the ClCrO plane, and the five-member product (**5**) from the [2+3] cycloaddition of C_2H_4 to the two terminal oxygens of CrO_2Cl_2. Distances are in angstroms and angles in degrees.

angles of ∠ClCrCl = 112.0° and ∠OCrCO = 108.7° are in line with the experimental findings[17c] of ∠ClCrCl = 113.3(3)° and ∠OCrCO = 108.5(4)°, respectively.

No symmetry was found for the [2+2] addition product, **4**, in which the four-membered CrOCC ring bisects the ClCrO angle. The coordination around chromium in **4** is square pyramidal with an axial Cr═O bond that is 0.01 Å shorter than the Cr═O linkages of CrO_2Cl_2. The second Cr−O bond has been stretched by 0.24 Å to 1.807 Å and the olefin C−C bond elongated to 1.485 Å as electron density from the former Cr−O double bond is donated into the π^* orbital of ethylene. To ensure that this conformation represents a global minimum, we also examined another enantiomer of the [2+2] product **4**, Figure 2, in which the four-membered ring bisects the ClCrCl angle. This isomer, **6**, was computed to be a local minimum with an energy 16.0 kcal mol^{-1} above that of **4**.

The ester complex **5** has a d^2 electronic configuration as the metal center formally has been reduced by the [2+3] addition of ethylene. The ground state was found to be a triplet whereas the corresponding singlet with a similar optimized geometry was 20.5 kcal/mol higher in energy. The ester, **5**, possesses a single C_2 axis and a puckered Cr−O−C−C−O five-membered ring with a dihedral ∠C−O−O−C angle of 42°. The puckering reduces the steric interaction between hydrogens and oxygens on adjacent carbons by allowing for a staggered conformation of the C−H and C−O bonds, **5**. The addition of olefin increases the two Cr−O distances by 0.19 Å whereas the C−C olefin

(26) Gunnarson, O.; Lundquist, I. *Phys. Rev.* **1974**, *B10*, 1319.
(27) Vosko, S. H.; Wilk, L.; Nusair, M. *Can. J. Phys.* **1980**, *58*, 1200.
(28) Becke, A. D. *Phys. Rev. A* **1988**, *38*, 2398.
(29) (a) Perdew, J. P. *Phys. Rev. Lett.* **1985**, *55*, 1655. (b) Perdew, J. P. *Phys. Rev. B* **1986**, *33*, 8822. (c) Perdew, J. P.; Wang, Y. *Phys. Rev. B* **1986**, *33*, 8800.
(30) (a) Deng, L.; Ziegler, T. *Organometallics* **1996**, *15*, 3011. (b) Ziegler, T.; Li, J. *Organometallics* **1995**, *14*, 214.
(31) (a) Versluis, L.; Ziegler, T. *J. Chem. Phys.* **1988**, *88*, 322. (b) Fan, L.; Ziegler, T. *J. Chem. Phys.* **1991**, *95*, 7401. (c) Schreckenbach, G.; Li, J.; Ziegler, T. *Int. J. Quantum Chem.* **1995**, *56*, 477.
(32) Fan, L.; Versluis, L.; Ziegler, T.; Baerends, E. J.; Ravenek, W. *Int. J. Quantum Chem. Symp.* **1988**, *22*, 173.
(33) (a) Ziegler, T.; Tschinke, V.; Baerends, E. J.; Snijders, G. J.; Ravenek, W. *J. Phys. Chem.* **1989**, *93*, 3050. (b) Schreckenbach, G.; Ziegler, T.; Li, J. *Int. J. Quantum Chem.* **1995**, *56*, 477.
(34) Banerjee, A.; Adams, N.; Simons, J.; Shephard, R. *J. Phys. Chem.* **1985**, *89*, 52.
(35) Baker, J. *J. Comput. Chem.* **1986**, *7*, 385.
(36) Fan, L.; Ziegler, T. *J. Chem. Phys.* **1990**, *92*, 46.
(37) Fukui, K. *Acc. Chem. Res.* **1981**, *14*, 363.
(38) González, C.; Schlegel, H. B. *J. Phys. Chem.* **1990**, *94*, 5523.
(39) Deng, L.; Ziegler, T. *Int. J. Quantum Chem.* **1994**, *52*, 731.

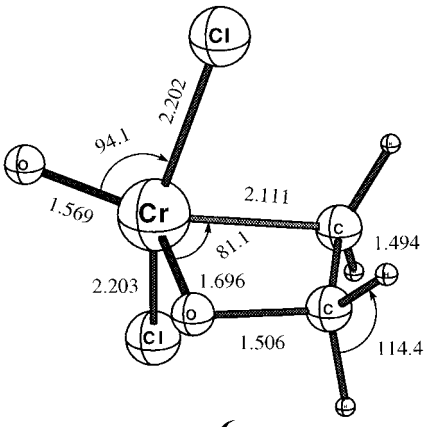

6

Figure 2. Optimized structure of the four-member product (**6**) from the [2+2] cycloaddition of C_2H_4 to the Cr═O bond of CrO_2Cl_2 in the OCrO plane. Distances are in angstroms and angles in degrees.

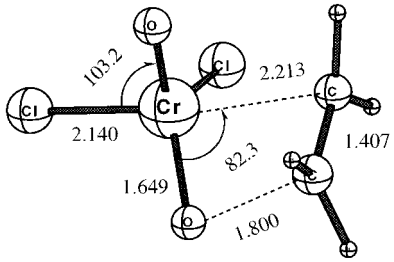

TS_1

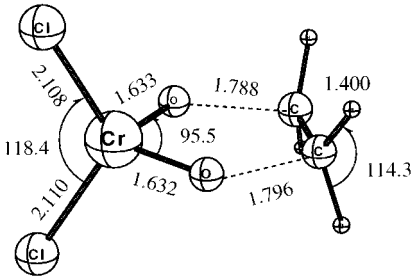

TS_2

Figure 3. Optimized geometries of the transition states for the [2+2] (**TS_1**) and [2+3] (**TS_2**) cycloaddition reactions between CrO_2Cl_2 and C_2H_4. Bond lengths are in angstroms and bond angles in degrees.

bond is stretched by 0.17 Å, again as a result of donation from the former Cr−O double bond into the π^* orbital of ethylene.

B. Transition State Structures. Figure 3 depicts the transition state (TS) structures for the [2+2] path of eq 1, **TS_1**, and the [2+3] path of eq 2, **TS_2**. The optimized TS's for the osmium system,[17a] **TS_3** and **TS_4**, are displayed in Figure 4 for comparison. Calculations of the energy Hessians revealed a single negative eigenvalue for each of these TS's

As illustrated in Figures 3 and 4, the geometries of the five-center TS's are quite similar for both chromium, **TS_2**, and osmium, **TS_4**. The atoms in the five-center framework are coplanar, with the O−C−C−O torsion angles being less than 10°. The osmium system, **TS_4**, represents an earlier transition state with a long C−O distance of 2.045 Å compared to the chromium transition state, **TS_2**, in which the C−O distance is reduced to 1.796 Å. By comparison, the C−O distances in the final products are 1.431 Å (Os) and 1.421 Å (Cr).

The optimized four-center TS's show slightly different geometries for the two metals. Thus, the M−O−C−C torsion angle is 25° for chromium, **TS_1**, and 8° for osmium, **TS_3**. We

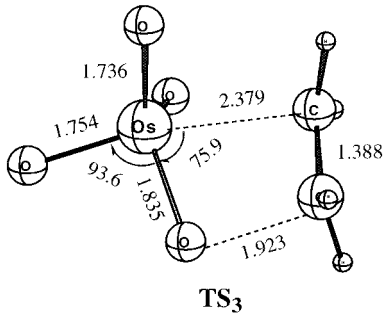

TS_3

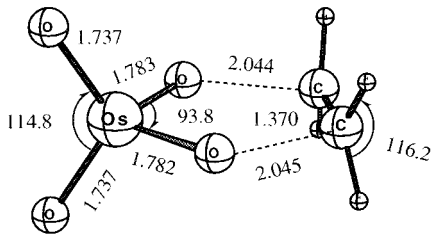

TS_4

Figure 4. Optimized geometries of the transition states for the [2+2] (**TS_3**) and [2+3] (**TS_4**) cycloaddition reactions between OsO_4 and C_2H_4. Bond lengths are in angstroms and bond angles in degrees.

note further that the C−C distances are stretched more in the chromium systems, **TS_1** and **TS_2**, than in the osmium systems, **TS_3** and **TS_4**, as in the case of the products.

The energy profiles for the [2+2] and [2+3] addition reactions along the IRC are shown at the bottom of Figures 5 and 6, respectively. The corresponding energy profiles for the osmium systems have been reported previously.[17a] It follows from Figure 5 that the [2+2] addition of ethylene to CrO_2Cl_2 is endothermic by 15.5 kcal/mol with an activation barrier of 27.9 kcal/mol.

The IRC energy profile, Figure 6, for the [2+3] cycloaddition of ethylene to CrO_2Cl_2 reveals that the process is exothermic by −9.6 kcal/mol and has an activation barrier of 15.8 kcal/mol. The [2+3] cycloaddition involves a formal reduction of the metal center from a d^0 to a d^2 configuration. The d^2 configuration gives rise to a triplet state in the case of chromium with the result that the reaction energy profile in Figure 6 displays a crossover from a d^0 singlet surface on the reactant side to a d^2 triplet surface on the product side. We shall discuss this in more detail later.

C. Intrinsic Reaction Paths for the Chromium System. The IRC method affords a steepest descent path in mass-weighted Cartesian coordinates from the TS toward reactants and products. We have already discussed the energy profile along this path given in Figures 5 and 6. We shall in the following discuss changes in the internal coordinates along the IRC path for the chromium systems. A similar discussion has been presented elsewhere[17a] for the osmium systems

Figure 5 (top) displays changes in internal coordinates along the IRC for the [2+2] cycloaddition, eq 1. The corresponding plot for the [2+3] cycloaddition of eq 2 is given in Figure 6. The IRC parameters represent in absolute terms the length of the path from the TS. A negative value characterizes the reactant path whereas the position on the product path is given by a positive value of *s*.

The IRC in Figure 5 was constructed from a total of 170 steps. It shows that the reaction proceeds in three stages. First, from the reactants ($s = -15$) to the vicinity ($s = -2$) of **TS_1**, ethylene initially attacks the Cr═O linkage in a nucleophilic

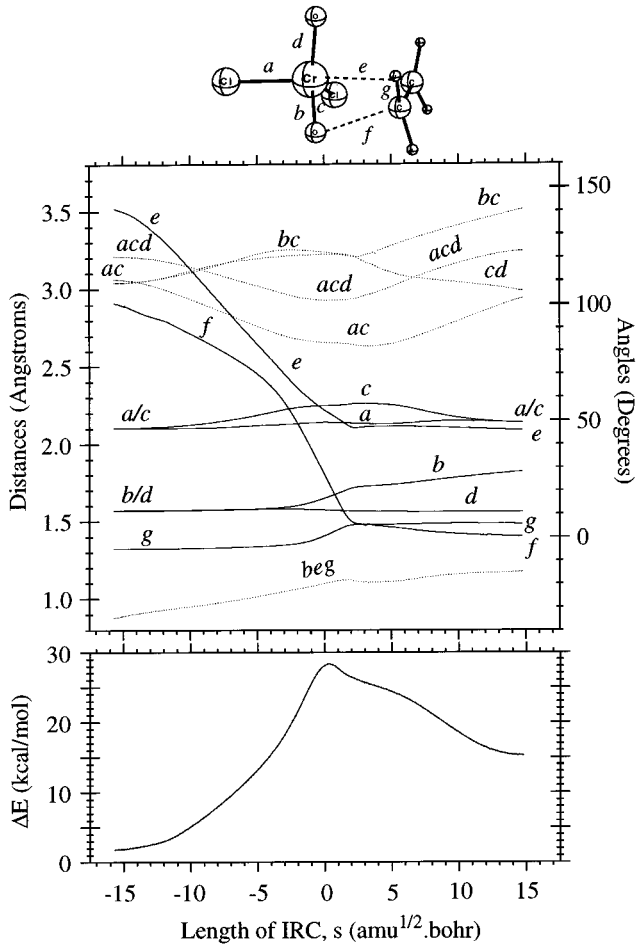

Figure 5. Changes in internal coordinates and energy for the chromium-catalyzed [2+2] cycloaddition reaction along the IRC path. The length of the IRC is given by s (amu$^{1/2}$•bohr). The transition state is at $s = 0.0$, the cycloaddition product is at $s \approx 15$, and the reactants $CrO_2Cl_2 + C_2H_4$ are at $s \approx -15$. Energies are relative to $CrO_2Cl_2 + C_2H_4$.

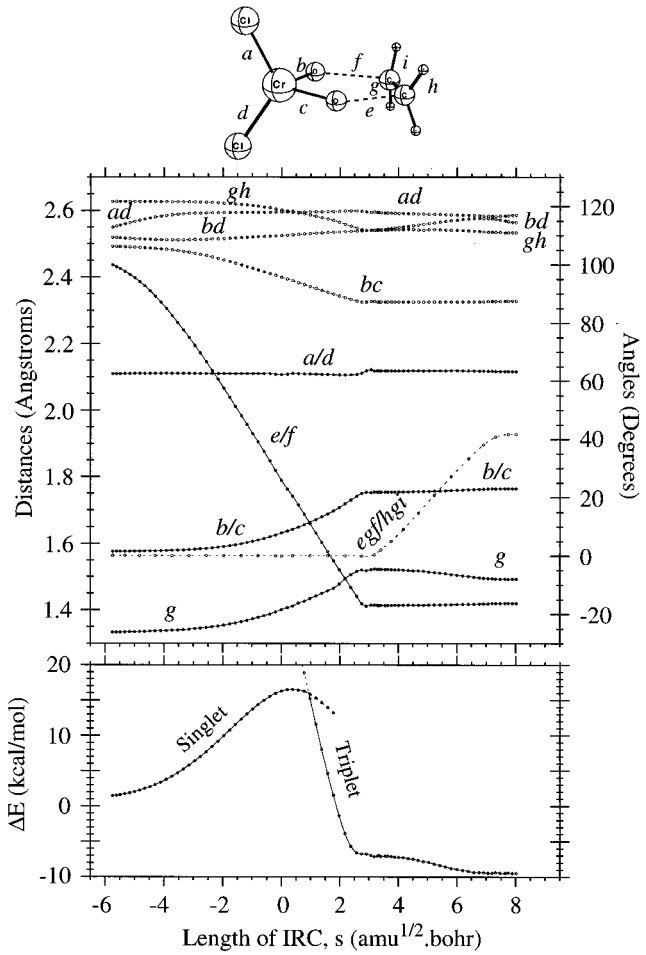

Figure 6. Changes in internal coordinates and energy for the chromium-catalyzed [2+3] cycloaddition reaction along the IRC path. The length of the IRC is given by s (amu$^{1/2}$•bohr). The transition state is at $s = 0.0$, the cycloaddition product is at $s \approx 8$, and the reactants $CrO_2Cl_2 + C_2H_4$ are at $s \approx -6$. Energies are relative to $CrO_2Cl_2 + C_2H_4$.

fashion. One of the carbon atoms moves gradually closer to the metal center and the empty chromium-based d orbitals. A linear decrease in the distance depicted by *e* of Figure 5 (top) facilitates the donation of electron density from the olefinic bond to the metal center. At this stage, neither *R*(C═C) (*g*) nor *R*(Cr═O) (*b* and *d*) has started to elongate. Also, the C−O distance (*f*) is still too long for an effective interaction. Up to this point in the path, the C−Cr bond formation is clearly ahead of the C−O bond making, as seen from comparing *e* and *f*. Thus, the *R*(C−Cr) distance has shortened nearly 1.0 Å, whereas the length of the C−O interaction has decreased by less than 0.5 Å.

The second stage occurs in the TS region, where the most remarkable change taking place is the acceleration of the C−O bond making (the slope for *f* becomes more negative than before and, in absolute terms, larger than for *e*). Simultaneously, two bond-breaking processes begin: on one hand, the olefin starts losing its double bond character (*g*); on the other hand, the Cr═O bond (*b*) is weakened as the oxygen atom starts a nucleophilic attack on the other olefinic carbon (*f*). The bond breaking is compensated for by the formation of the C−O linkage (*f*) and the completion of the C−Cr bond (*e*).

Few structural changes occur in the last stage, $s = 2-15$, of the reaction. Here, both *e* and *g* remain constant. As *f* slowly converges to the product C−O distance, *b* increases at the same rate. We note finally that the ∠OCrCl angle *bc* increases throughout the reaction from 109 to 145° in order for the final product to attain its square pyramidal conformation with one oxygen in an axial position, **4**.

Let us turn now our attention to the pathway leading to a five-member intermediate. For the [2+3] cycloaddition, the reaction path of lowest energy (Figure 6) involves a crossover from the singlet surface to the triplet surface once the TS has been past. The IRC was traced on the singlet PES in the first place since the TS is situated here. The singlet energies were calculated at each IRC point from the TS toward the product until a crossing point was found at $s = 1.0$ where the singlet−triplet energy splitting is less than 0.1 kcal mol^{-1}. From this point, the true IRC was approximately represented by the steepest descent path on the triplet PES down to the triplet product in the mass-weighted Cartesian coordinate system. A total of 80 steps were computed.

As illustrated, tracing the IRC path on the lowest energy surface for the reaction in eq 2 reveals that **TS_2** connects on the product side to the local minimum **5**, which is 11.4 kcal mol^{-1} more stable than the corresponding product on the singlet PES. The reactant and the transition state, **TS_2**, both have an electronic singlet ground state in accordance with the formal d^0 configuration on the metal center.

Conceptually, such a crossing would be made possible by spin−orbit coupling. Spin−orbit interactions are the main cause for the breakdown of the selection rule that forbids intersystem

crossing. The greater the spin−orbit coupling is, the greater the probability that the spin change occurs at or near the crossover point of the two different energy surfaces. Spin−orbit coupling increases with the principal quantum number; it is relatively small for light main group elements, resulting in a high level of adiabaticity in organic systems, but it is much greater for TM complexes. Therefore, it is expected that reactions involving organometallic species are highly adiabatic.[41]

The natural reaction coordinate for the [2+3] cycloaddition is the R(C−O) distance (*e* or *f*) which shrinks linearly with *s* from 2.44 Å at $s = -6.0$ to 1.42 Å at the flat end region of the energy profile. The first half of the reaction path up to the transition state **TS2** is marked by very small changes in the other coordinates except for an increase in the ClCrCl angle *ad*. After the transition state **TS2** has been reached, the proper formation of the five-member ring begins. Thus, a closure of the OCrO bond angle (*bc*) takes place simultaneously with the elongation of the Cr═O linkages (*b*/*c*) and the C−C bond (*g*). The C−O bond making more than compensates for the Cr−O and C−C bond stretching as the energy decreases. Interestingly, the crossing point occurs just immediately after the highest point in energy ($s = 1.0$), but none of the structural parameters turn out to exhibit any abrupt change after the crossover from the singlet to the triplet potential energy surface.

The last stage ($s > 2.3$) of the reaction path is characterized by the loss of the planarity of the five-membered ring. As seen from Figure 6, the *egf* torsion angle changes from 0 to 42°. Such a distortion serves to relieve angle strain. It also reduces the steric interaction between C−H bonds on adjacent carbon centers (*hgi* dihedral angle). A similar reduction is achieved for the steric interaction between the two C−O bonds (*egf*). Notice, however, that the gain in stability from $s = 2.2$ to $s = 8.0$ (**5**) is only 3 kcal/mol.

D. Comparison of Reactivity Patterns for CrO_2Cl_2 and OsO_4. The calculated reaction enthalpies and activation energies for the [2+2] and [2+3] cycloaddition of ethylene to OsO_4 and CrO_2Cl_2 are summarized in Figure 7. All energies are relative to the separate reactants.

It is clear from Figure 7 that the [2+3] addition is preferred over the [2+2] process for both metal systems. Thermodynamically, the [2+3] reaction is favored by 24.3 kcal/mol for OsO_4 compared to 25.0 kcal/mol in the case of CrO_2Cl_2. Kinetically, the [2+3] addition is characterized by barriers of 1.8 and 15.8 kcal/mol for OsO_4 and CrO_2Cl_2, respectively, whereas much higher activation energies of 39.7 and 27.9 kcal/mol, respectively, are found for the [2+2] addition.

We shall now turn to a qualitative analysis of the trends summarized in Figure 7, starting with the [2+3] addition. A previous discussion has been given by Jørgensen and Hoffmann[42] based on the extended Hückel method.

E. Analysis of the [2+3] Addition Reaction. The orbital levels for the CrO_2Cl_2 reactant have been established by photoelectron spectroscopy[43a] and theoretical calculations.[43b] Similar experimental[43c] and theoretical[43d] investigations have been carried out on OsO_4.

The [2+3] addition of ethylene to two oxygens on OsO_4 or CrO_2Cl_2 involves primarily three occupied, **7a**−**c**, and two

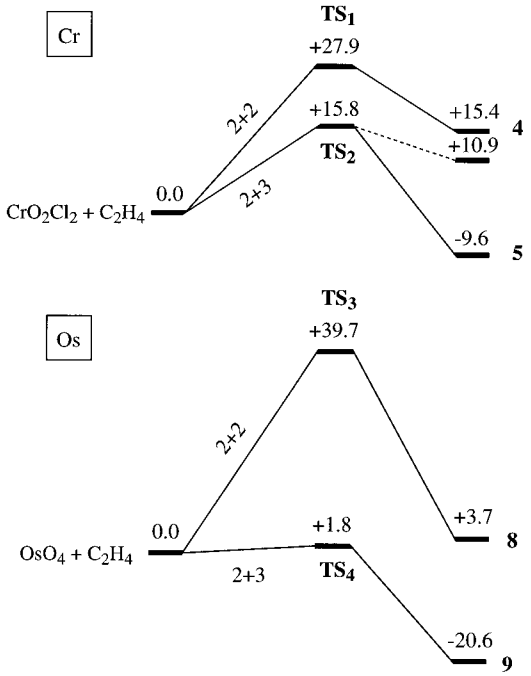

Figure 7. Schematic representation of the energetics involved in the [2+2] and [2+3] cycloaddition reactions for the CrO_2Cl_2 (above) and OsO_4 (below) systems. Energies are in kcal mol^{-1}.

unoccupied, **7d**,**e**, orbitals. The electron pairs in the two oxygen-

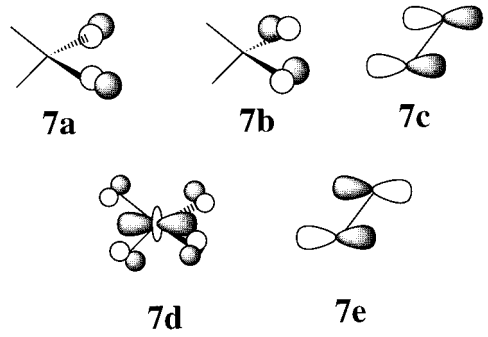

based orbitals, **7a**,**b**, are stabilized throughout the reaction by in-phase contributions from the ethylene π, **7c**, and π^*, **7e**, orbitals, respectively, to form the two C−O bonding orbitals **8a** and **8b**. However, the third electron pair originally residing

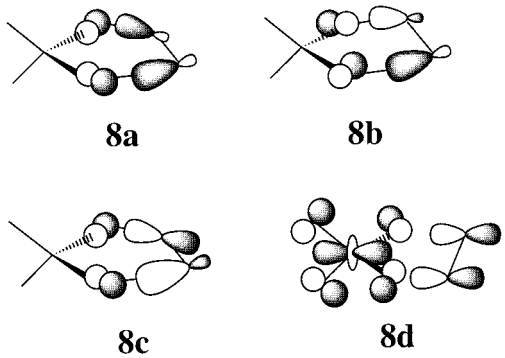

in the ethylene π orbital, **7c**, will initially be destabilized as it occupies the out-of-phase combination, **8c**, between π, **7c**, and the oxygen-based lone pair **7a**. The destabilization could potentially lead to a substantial activation barrier and an endothermic reaction enthalpy. Fortunately, the LUMO, **7d**, on either CrO_2Cl_2 or OsO_4 has a (bonding) overlap, **8d**, with π

(40) Rondan, N. G.; Houk, K. N. *J. Am. Chem. Soc.* **1985**, *107*, 2099.
(41) Poli, R. *Chem. Rev.* **1996**, *96*, 2135.
(42) Jørgensen, K. A.; Hoffmann, R. *J. Am. Chem. Soc.* **1986**, *108*, 1867.
(43) (a) Lee, T. H.; Rabalias, J. W. *Chem. Phys. Lett.* **1975**, *34*, 135. (b) Ziegler, T. Ph.D. Thesis, University of Calgary, 1978. (c) Foster, S.; Felps, D.; Cusachs, I. C. McGlynn, S. P. *J. Am. Chem. Soc.* **1973**, *95*, 5521. (d) Rauk, A.; Ziegler, T.; Ellis, D. E. *Theor. Chim. Acta* **1974**, *34*, 49.

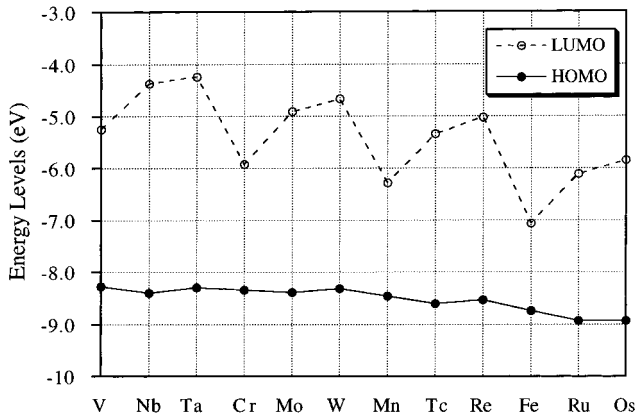

Figure 8. Energies of highest occupied and lowest unoccupied orbitals in the tetrahedral d^0 metal complexes with the formulas $MO_{4-n}Cl_n$ [M = V, Nb, Ta ($n = 3$); M = Cr, Mo, W ($n = 2$); M = Mn, Tc, Re ($n = 1$); M = Fe, Ru, Os ($n = 4$).

in **8c**, which initially will help reduce the barrier and eventually facilitate a transfer of the electron pair from the rising antibonding orbital **8c** to the metal-centered LUMO, **7d**. Thus the LUMO **7d** has a crucial role in initially stabilizing the electron pair of **8c** and ultimately will completely accept it.

We have previously considered the one-electron reduction process

$$MO_{4-n}Cl_n + H \rightarrow MO_{3-n}Cl_n(OH) \qquad \Delta H_5 \qquad (5)$$

in which the d^0 metal center changes to a d^1 configuration. We were able to show[30a] that the calculated heat of reaction followed the trend in the energy of the $MO_{4-n}Cl_n$ LUMO, **7d**, shown in Figure 8. Thus, within a triad, the process becomes less exothermic from top to bottom as the LUMO rises in energy due to the usual increase in the antibonding ligand−metal interaction. Also, within a transition series, the reaction becomes more exothermic from left to right as the LUMO drops in energy with increasing electronegativity of the metal center (and the surrounding ligands).

We expect the heat of reaction for the [2+3] cycloaddition of ethylene to terminal oxygens on $MO_{4-n}Cl_n$

$$MO_{4-n}Cl_n + C_2H_4 \rightarrow MO_{2-n}Cl_nO_2C_2H_4 \qquad \Delta H_6 \quad (6)$$

to follow the same trend due to its status as a two-electron reduction process. Thus, the addition of C_2H_4 to WO_2Cl_2 should be less favorable than that to CrO_2Cl_2 or $ReClO_3$.

The magnitude of the barrier for the [2+3] addition reaction is inversely proportional to the size of the overlap, **8d**, between the ethylene π orbital, **7c**, and the LUMO, **7d**. The overlap will further increase with the oxygen contribution to **7d**. Chromium is less electronegative than osmium with a smaller oxygen composition in **7d**. As a consequence, the [2+3] activation barrier is larger for CrO_2Cl_2 than for OsO_4, Figure 8. We expect the barrier to decerease substantially from left to right in a transition series and to a lesser extent from top to bottom in a triad.

F. Analysis of the [2+2] Addition Reaction. The [2+2] addition of ethylene to the metal−oxygen bond in OsO_4 or CrO_2Cl_2 involves primarily two occupied, **7c** and **9a**, and two unoccupied, **7d**,**e**, orbitals. One electron pair residing in the oxygen-based orbital **9a** is stabilized by π of ethylene to form the C−O bonding orbital **9b**. At the same time the second

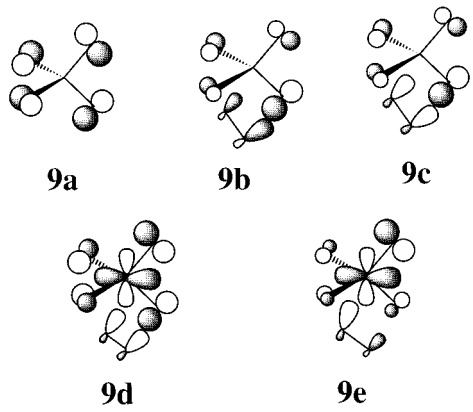

electron pair in π of ethylene, **7c**, is destabilized, **9c**, in the out-of-phase interaction with the oxygen-based orbital **9a**.

In the corresponding [2+3] addition reaction, the energy rise of π was effectively prevented by a stabilization "from above" by the empty LUMO orbital, **7d**, due to a large, **8d**, π-type overlap between 7**c** and **7d**. The overlap, **9d**, between π and **7d** is much less favorable in the [2+2] approach, where **7d** now acts as a π^*-rather than π-type orbital. For this reason the energy of the electron pair in **9c** is allowed to rise, resulting in a substantial barrier. Eventually the much higher lying π^* orbital, **7e**, of ethylene will mix into the olefin orbital and polarize it toward the d lobe of **7d**. This polarization eventually gives rise to the Os−C bonding orbital **9e**. Thus, the formation of the Os−C bond requires the admixture of two vacant orbitals on different fragments, **7d** and **7e**.

In the [2+3] addition, the large (50%) contribution from oxygen to the LUMO of OsO_4 was instrumental in a substantial overlap with π, **8d**, and a low barrier. In the [2+2] addition, the equal mix of oxygen reduces the overlap between π and **7d**, **9d**, and increases the barrier. For CrO_2Cl_2, where the d contribution in **7d** is predominant, the overlap **9d** is better and the barrier lower, Figure 8. However, for both systems the [2+3] approach is favored over the [2+2] addition because the stabilizing overlap between π and the metal-based LUMO, **7d**, is larger in the former process, **8d**, compared to the latter, **9d**.

Concluding Remarks

We have shown from DFT calculations that the [2+3] addition of ethylene to metal−oxygen bonds in CrO_2Cl_2 and OsO_4 are favored over the [2+2] addition to a M=O linkage both kinetically and thermodynamically. The calculated differences are much larger than the error margin of 5 kcal/mol associated with the DFT scheme applied here. It is concluded that epoxides formed in the reaction between CrO_2Cl_2 and olefins are unlikely to originate from a [2+2] addition path to a Cr=O bond. We expect to explore alternative pathways for the formation of epoxides in a later investigation. A qualitative analysis of the [2+3] addition to metal−oxygen bonds in tetrahedral d^0 MO_nCl_{4-n} complexes ($n = 2-4$) leads to the prediction that the exothermicity should increase from bottom to top in a triad and from left to right in a transition series. It was further shown that the [2+3] addition process has a relative low barrier due to a good π-type overlap between the ethylene π orbital and the LUMO on the metal complex. The barrier will be especially low for d^0 oxo complexes with a covalent (rather than a polar) bond, as in the case of OsO_4. The qualitative analysis of the [2+2] addition to a M=O linkage underlined that this process has a high barrier due to a poor

overlap between the ethylene π orbital and the LUMO on the metal complex since the LUMO acts as a π^* orbital in the [2+2] approach with a nodal plane through the M═O bond.

Acknowledgment. This investigation was supported by the Natural Sciences and Engineering Research Council of Canada (NSERC), as well as the donors of the Petroleum Research Fund, administered by the American Chemical Society (ACS-PRF Grant No. 31205-AC3). We also acknowledge access to the computer facilities at the universities of Calgary and Girona. M.T. thanks the Direcció General de Recerca de la Generalitat de Catalunya for financial help through an FI Fellowship.

IC970896H